J Therm Anal Calorim (2014) 116:655–662
DOI 10.1007/s10973-013-3489-1

Crystal structure, thermal behavior, and microbiological activity of a thiosemicarbazide-type ligand and its cobalt complexes

Berta Holló · Marko V. Rodić · Ljiljana S. Vojinović-Ješić · Vukosava Živković-Radovanović · Gordana Vučković · Vukadin M. Leovac · Katalin Mészáros Szécsényi

Received: 22 July 2013 / Accepted: 18 October 2013 / Published online: 12 November 2013
© Akadémiai Kiadó, Budapest, Hungary 2013

Abstract The synthesis of a potentially bioactive mixed-valence Co^{III}/Co^{II} complex with 2-acetylpyridine *S*-methylisothiosemicarbazone (**HL**) ligand is described. The crystal and molecular structure of the formed $[Co^{III}L_2][Co^{II}Cl_3py]\cdot Me_2CO$ (**I**) compound (*py* stands for pyridine) is determined by single-crystal X-ray crystallography. It's thermal decomposition along with the decomposition of the ligand and six structurally related complexes with formulas $[CoL_2]NO_3\cdot MeOH$ (**1**), $[CoL_2]Br\cdot MeOH$ (**2**), $[CoL_2]HSO_4\cdot MeOH$ (**3**), $[CoL_2]_2[Co^{II}(NCS)_4]$ (**4**), $[Co(HL)(L)]I_2\cdot 2MeOH$ (**5**), and $[Co(HL)(L)][Co^{II}Cl_4]\cdot MeOH$ (**6**) was determined by simultaneous TG/DSC measurements. The decomposition pattern is evaluated using TG/DTA-MS data. The results were related to the solvent/moisture content and the decomposition mechanism of the compounds. The antimicrobial activity of the ligand and of all the complexes was tested in vitro for selected gram-negative and gram-positive bacteria and fungi. The activity of the ligand against all tested bacteria is comparable with those obtained for standard antibiotics, while it is less active against fungi. Surprisingly, the activity of the complexes is very low. The low antimicrobial activity of the complexes may be in connection with their high thermodynamic and kinetic inertness in solution. The results are also supported by the relatively high thermal stability of the complexes.

B. Holló · M. V. Rodić · L. S. Vojinović-Ješić · V. M. Leovac · K. M. Szécsényi (✉)
Faculty of Sciences, University of Novi Sad, Trg Dositeja Obradovića 3, 21000 Novi Sad, Serbia
e-mail: mszk@uns.ac.rs

V. Živković-Radovanović · G. Vučković
Faculty of Chemistry, University of Belgrade, P.O. Box 51, 11158 Belgrade, Serbia

Keywords Co^{III} and mixed-valence Co^{III}/Co^{II} complex · 2-Acetylpyridine *S*-methylisothiosemicarbazone · TG/DSC · EGA–MS · Biological activity

Introduction

A high-frequency occurrence of drug-resistant microbial strains [1, 2] implies intensive research for new antimicrobial agents. One of the possibilities to enhance the pharmacological potency of already used drugs is their complexation with metals [3, 4]. Complex formation alone often results in increased biological activity [5] in the obtained compounds. The metal ion coordinated within the active site can block the enzymatic activity, thus inhibiting interactions with the biological substrates [6, 7]. Studying the chelating preferences of pharmacophores is one of the tools used in effective drug design.

Thermal analysis is one of the most frequently used techniques in pharmaceutical industry applied from testing of new compounds with potential biological activity, crystal morphology studies [8, 9], and assessment of possible incompatibility between the active component and different excipients [10, 11], to quality control of final products [12, 13].

Transition metal complexes with Schiff base ligands are known for their pronounced bioactivity [14–16]. On coordination with metal ions some macrocyclic Schiff bases showed a considerable enhancement in antifungal activity against selected fungal strains [17]. Complex formation of Co^{II} with 3-salicylidene-hydrazono-2-indolinone increased the antimicrobial and anti-inflammatory effect of the ligand [18]. It was also found that heterometallic systems show

synergistic effect of the two metals [19, 20] concerning the cytotoxicity. As in principle both Co^{II} and Co^{III} complexes exhibit antimicrobial activity [21–23]; one of the aims of the study was to see how the oxidation state of the central ion affects the antimicrobial activity of the compounds.

In our previous paper we described the synthesis and crystal structure of six potentially bioactive cobalt(III) complexes with 2-acetylpyridine *S*-methylisothiosemicarbazone (**HL**) of formulas $[CoL_2]NO_3{\cdot}MeOH$ (**1**), $[CoL_2]Br{\cdot}MeOH$ (**2**), $[CoL_2]HSO_4{\cdot}MeOH$ (**3**), $[CoL_2]_2[Co^{II}(NCS)_4]$ (**4**), $[Co(HL)(L)]I_2{\cdot}2MeOH$ (**5**), and $[Co(HL)(L)][Co^{II}Cl_4]{\cdot}MeOH$ (**6**), as well as of **HL** [24]. In this paper we report the synthesis and structure of the new $[CoL_2][Co^{II}Cl_3py]{\cdot}Me_2CO$ (**I**) compound (*py* stands for pyridine) with its antimicrobial activity against selected microbial strains along with antimicrobial activity of the former complexes. As the thermal stability may be crucial to assessing applicability of new compounds, the thermal behavior of the ligand and the complexes is discussed in detail.

Experimental

Synthesis of $[Co^{III}L_2][Co^{II}Cl_3py]{\cdot}Me_2CO$ (**I**): **HL** (104 mg; 0.5 mmol) was dissolved in Me_2CO (10 cm^3) and to the pale-yellow solution pyridine (1 cm^3; 1.33 mmol) was added, which was then mixed with solution of $CoCl_2{\cdot}6H_2O$ (238 mg; 1 mmol) in Me_2CO (5 cm^3). The reaction mixture was left to evaporate slowly at room temperature for 3 days. The formed dark-green single crystals were filtered off. Yield: 170 mg.

The synthesis of the ligand and the compounds **1**–**6** is described elsewhere [24].

Thermal data were collected using TA Instruments SDT-Q600 TGA/DSC equipment at 10 °C min^{-1} heating rate in N_2 atmosphere (sample mass: ~3 mg), while TG/DTA-MS data were collected using TA Instruments SDT 2960 DTA/TGA online coupled with Balzers Instruments ThermoStar GSD 300T quadrupole mass spectrometer also at 10 °C min^{-1} heating rate and in N_2 atmosphere (flow rate 130 cm^3 min^{-1}). Selected ions between m/z = 1–129 were monitored through 64 channels in Multiple Ion Detection Mode (MID) with a measuring time of 0.5 s per channel.

Diffraction data for complex **I** were collected on a Gemini S κ-geometry diffractometer (Agilent Technologies). A single crystal of the complex **I** was selected, glued on glass fiber, and mounted on the goniometer. Sealed tube with Mo-anode was used as a source of X-radiation, which was monochromatized by a graphite crystal (Mo $K\alpha$, λ = 0.71073 Å). Diffraction pattern obtained by ω scan method was recorded with Sapphire3 CCD area detector. Data collection, reduction, absorption correction (multi-scan), and cell refinement were performed with the CRYSALISPRO [25]. Structure was solved by direct method implemented in SIR92 [26]. The model was refined with the SHELXL-2013 program [27] using the least squares minimization. SHELXLE [28] was used as graphical user interface for refinement data manipulation. H atoms bonded to C atoms were placed at calculated positions and refined using riding model, while H atoms attached to N atoms were located in a difference Fourier map and refined with their U_{iso} set as 1.2 U_{eq} of their parent atoms. Acetone molecule was refined with appropriate distance and ADP restraints. Structural data were validated and analyzed with PLATON [29]. The figure was produced using ORTEP-3 [30].

Crystal data $C_{26}H_{33}Cl_3Co_2N_9OS_2$, M = 775.94, monoclinic, $P2_1/c$, a = 13.0073(3) Å, b = 15.2840(4) Å, c = 18.0055(4) Å, β = 107.452(2)°, V = 3414.8(2) $Å^3$, Z = 4, 17830 reflections measured, 7826 unique (R_{int} = 0.031) which were used in all calculations. The final wR_2 was 0.139 (all data) and R_1 was 0.059 ($I > 2\sigma(I)$). Crystallographic data reported for the complex (**I**) have been deposited with CCDC, No. CCDC 931361. Copies of the data can be obtained free of charge via www.ccdc.cam.ac.uk.

The in vitro antimicrobial activity was tested for Gram-negative bacterium *Escherichia coli* ATCC 25922 (*E.C.*), Gram-positive bacteria *Staphylococcus aureus* ATCC 25923 (*S.A.*), *Bacillus subtilis* ATCC 6633 (*B.S.*), *Bacillus cereus* ATCC 14579 (*B.C.*), and *Micrococcus lysodeikticus* ATCC 4698 (*M.L.*), respectively, and for fungi yeast *Candida albicans* ATCC 24433 (*C.A.*), and mold *Aspergillus niger* ATCC 12066 (*A.N.*). The bacteria were cultivated on LAB 8 nutrient agar and fungi on LAB 37 malt extract agar. Bacteria were thermostated at 37 °C for 24 h and fungi at 28 °C for 48 h. All assays were performed by the method of diffusion in agar [31, 32]. Stock solutions of each compound (c = 4 mg cm^{-3}) in a solvent mixture of DMSO:H_2O = 1:9 were double diluted with distilled water to concentration of 2 μg cm^{-3}. For the minimum inhibitory concentrations (MIC) determination 0.1 cm^3 of solutions were introduced in ø10 mm holes in inoculated agar plates. Inoculation was performed by mixing 0.50 cm^3 of the test microorganism suspension in sterile physiological solution with 10 cm^3 of molten medium cooled down to 50 °C. After corresponding incubation the diameters of the obtained zones were measured.

Results and discussion

By complex formation **HL** stabilizes cobalt(III). Therefore, when choosing the reacting components we have taken into account that anions Cl^- and NCS^- have coordination preferences toward Co^{II} and by this way they may favor the formation of complex anions with Co^{II}. So, in reaction of

$CoCl_2$ and $Co(NCS)_2$ with **HL** compounds with complex anions $[CoX_4]^{2-}$, X = Cl^-, NCS^- (**4** and **6**, respectively) were obtained [24]. However, the complex cations in compounds **4** and **6** are different. In **4** both ligand molecules coordinate to Co^{III} in deprotonated form giving $[Co^{III}L_2]_2[Co^{II}(NCS)_4]$. In **6** only one of the **HL** is deprotonated as in reaction of CoI_2 and **HL**. The formation of $[Co^{III}(HL)(L)]^{2+}$ instead of $[Co^{III}L_2]^+$ may be explained by the dominance of soft–hard interactions between the cations and anions over steric factors. In synthesis of **I** beside Co^{II} chloride and the ligand, *py* as additional ligand was added. Due to its high basicity the deprotonation of the second ligand also occurs. So, instead of $[Co^{III}(HL)(L)]^{2+}$ cation $[Co^{III}L_2]^+$ is formed that crystallizes with $[Co^{II}pyCl_3]^-$ anion in form of $[Co^{III}L_2][Co^{II}pyCl_3]\cdot Me_2CO$ (**I**). By this way we prepared two series of compounds. Complexes **1**–**3** and **5** contain Co^{III} only, while in complexes **4**, **6**, and **I** cobalt appears in both Co^{III} and Co^{II} oxidation states.

Crystal and molecular structure of **I**

The molecular structure of **I** is presented in Fig. 1 while selected bond distances and angles for the complex are given in Table 1. The asymmetric unit of the unit cell contains complex cation $[Co^{III}L_2]^+$, complex anion $[Co^{II}Cl_3py]^-$, and crystalline acetone molecule.

Molecular structure of the complex cation is similar to those in compounds **1**–**3** as Co(III) is situated in a slightly deformed octahedral environment formed by six meridionally arranged nitrogen atoms from the two ligand molecules. The NNN tridentate coordination mode of the ligands via the pyridine, azomethine, and isothioamide nitrogen atoms, each forming two five-membered

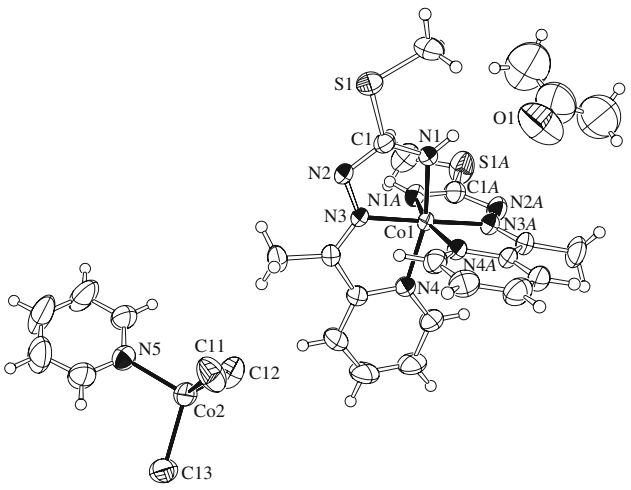

Fig. 1 Molecular structure of **I** with atom-numbering scheme for selected atoms. Displacement *ellipsoids* are drawn at the 50 % probability level

Table 1 Selected bond lengths and valence angles for **I**

Bond	Distance/Å	Bonds	Angle/°
Co1–N1	1.900(3)	N1–Co1–N4	163.9 (1)
Co1–N1*A*	1.916(3)	N1*A*–Co1–N4*A*	164.0 (1)
Co1–N3	1.868(3)	N3–Co1–N3*A*	178.2 (1)
Co1–N3*A*	1.869(3)	N1–Co1–N3	81.2 (1)
Co1–N4	1.944(3)	N1*A*–Co1–N3*A*	81.1 (1)
Co1–N4*A*	1.937(3)	N3–Co1–N4	82.9 (1)
Co2–Cl1	2.231(1)	N3*A*–Co1–N4*A*	82.8 (1)
Co2–Cl2	2.248(2)	Cl1–Co2–Cl2	115.85 (5)
Co2–Cl3	2.259(1)	Cl1–Co2–Cl3	113.52 (6)
Co2–N5	2.055(3)	Cl2–Co2–Cl3	111.28 (7)
N1–C1	1.306(4)	Cl1–Co2–N5	104.7 (1)
N1*A*–C1*A*	1.300(4)	Cl2–Co2–N5	106.0 (1)
C1–N2	1.349(4)	Cl3–Co2–N5	104.2 (1)
C1*A*–N2*A*	1.351(5)		
N2–N3	1.362(3)		
N2*A*–N3*A*	1.357(4)		
N3–C3	1.299(4)		
N3*A*–C3*A*	1.300(4)		

metallocycles, is expected and similar to that found in **1**–**6** [24]. Cobalt–ligator distances are in the range 1.868(3)–1.944(3) Å, where pyridine nitrogen atoms form the longest bonds, and the azomethine nitrogens the shortest ones, same as in compounds **1**–**6** [24]. Both ligand molecules are highly planar, in accordance with the conjugated system of double bonds in its backbone. **HL** coordinates in its imido form due to hydrogen migration from isothioamide nitrogen atom to hydrazine nitrogen atom, followed by its dissociation. The coordination and deprotonation of **HL** leads to structural changes comparable to those found for previously reported Co(III) and Cu(II) complexes [24, 33], *i.e.*, to shortening of N1–C1 and N1*A*–C1*A* bonds and elongation of C1–N2 and C1*A*–N2*A*, compared to those found in the free ligand [24].

Molecular structure of the complex anion $[Co^{II}Cl_3py]^-$ is distorted tetrahedral, in agreement with the affinity of Co(II) for tetrahedral coordination geometry. The Co(II)–chloride distances are similar in length [2.231(1)–2.259(1) Å], the Co2–N5 distance is shorter [2.055(3) Å] and as such are within expected values [34]. Angles Cl–Co2–Cl are significantly higher [111.28(7)–115.85(5)°] than Cl–Co2–N5 angles [104.2(1)–106.0(1)°], which is in line with stronger repulsion between negatively charged chlorido ligands. Geometrical parameters of $[Co^{II}Cl_3py]^-$ are comparable to those found in $[Co^{III}(L'')py_3][Co^{II}Cl_3py]$ (H_2L'' = salicylaldehyde semicarbazone) [35] and $[Co^{III}(L')py_3][Co^{II}Cl_3py]\cdot EtOH$ (H_2L' = salicylaldehyde *S*-methylisothiosemicarbazone) [36].

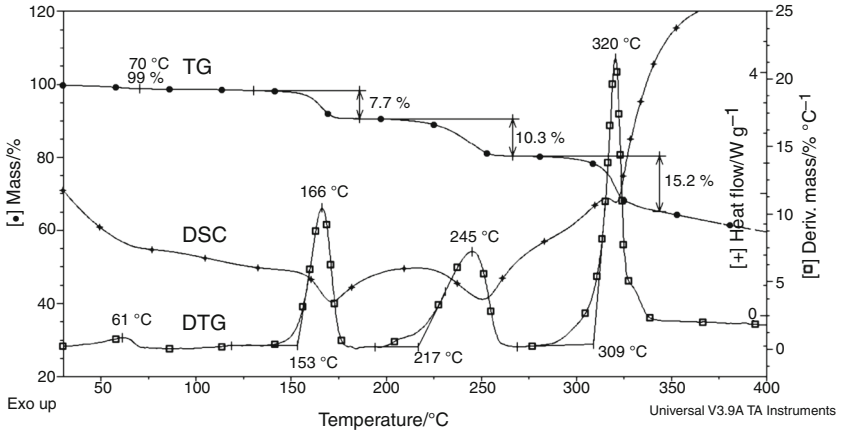

Fig. 2 TG, DTG, and DSC curves for compound **I**

Besides ionic interaction, association of the molecules in the solid state is determined by the presence of two hydrogen bonds. Namely, hydrogen bond N1*A*–H1*A*···N2^{i} [symmetry code: (i) $-x$, $-y$, $-z+1$] connects cations in centrosymmetric dimers, a motif also characteristic for compounds **1**–**6**. Acetone molecule is bonded to the complex cation via N1–H1···O1^{ii} [symmetry code (ii) $-x$, $-½+y$, $-z+½$] hydrogen bond of a moderate strength. Geometrical parameters of these secondary interactions are: d(N1*A*···N2^{i}) = 3.118(4) Å, ∠(N1*A*–H1*A*···N2^{i}) = 164(4)°; d(N1···O1^{ii}) = 3.145(6) Å, ∠(N1–H1···O1^{ii}) = 147(3)°.

Thermal analysis

The ligand melts at 89.1 °C onset. The melt is stable to 170 °C onset and in the temperature range of 200–350 °C 90 % of **HL** decomposes by slightly exothermic reactions. In nitrogen at 700 °C about 4 % tar residue is left.

As all the complexes except **4** are solvates the decomposition starts with solvent evaporation. TG curves reveal a steady solvent evaporation beginning at room temperature up to decomposition onset temperature of the complex. The mass loss found in **1**, **3**, and **5**–**6** is less than the half of the calculated MeOH content. Even in freshly prepared samples the amount of MeOH is somewhat less than the calculated one.

On the contrary, compound **I** is stable to 150 °C which seems too high temperature for acetone evaporation (boiling point: 56.1 °C or 329.3 ± 0.3 K [37]; Δm – exp: 7.7 %, calcd: 7.49 %) but is not without exception [38]. After acetone removal, [Co^{III}L$_2$][Co^{II}Cl$_3$*py*] is stable to around 200 °C and in the next decomposition step it loses pyridine (exp: 10.3 %, calcd: 10.19 %). The formed Co$_2^{III/II}$L$_2$Cl$_3$ (**II**) is also stable to ~300 °C. Its decomposition continues with HCl departure (exp: 5.5 %, calcd: 5.18 %) determined by precipitation reaction between Ag^+ and Cl^- when of the evolved gases bubble through an acidic solution of $AgNO_3$. The thermal curves of compound **I** are presented in Fig. 2.[1]

The decomposition of the desolvated complexes containing cobalt(III) only (**1**–**3** and **5**) starts at 173 °C onset in **5**, and have a stability order of **5** < **2** < **1** < **3** (166 < 191 < 245 < 261 °C). The thermal stability of compounds with both Co^{II} and Co^{III} is in the same temperature range and increases in order of **4** < **I** < **6** (186 < 217 < 249 °C). The mechanism of the decomposition for compounds **1** – **6** is presented by the corresponding DTG curves in Fig. 3.

Mechanism of decomposition

To elucidate the mechanism of decomposition, evolved gas analysis (EGA) of the decomposition was performed by coupled TG/MS measurements.

The decomposition of the ligand (**HL**, presented in Scheme 1) at the highest decomposition rate is accompanied by evolution of the fragments with m/z values of 47, 48, and 79 (see data in Table 2) belonging to species of CH_3S^+, CH_3SH^+, and $C_5H_5N^+$ (*py*), respectively. The origin of the fragment with $m/z = 64$ appearing below 300 °C in all the complexes, too, is questionable. In principle, it could belong either to CH_3CH_2Cl, to SO_2 or S_2 formation. As neither Cl nor O atoms are present in **HL** or in all the samples and the decomposition is monitored in the inert atmosphere of N_2, the peak may be the result of S_2 formation as was found in compounds containing sulfur [39–41]. This supposition is supported by the fact that the decomposition is endothermic in the measured range except for **1** containing nitrate ion, where the decomposition is exothermic in the range of 250–300 °C and is accompanied by water evolution ($m/z = 18$) and in **I** by exothermic reactions above 350 °C (see Fig. 2). The

[1] The freshly prepared **I** contains about 1 % of adsorbed acetone that during storage completely evaporates.

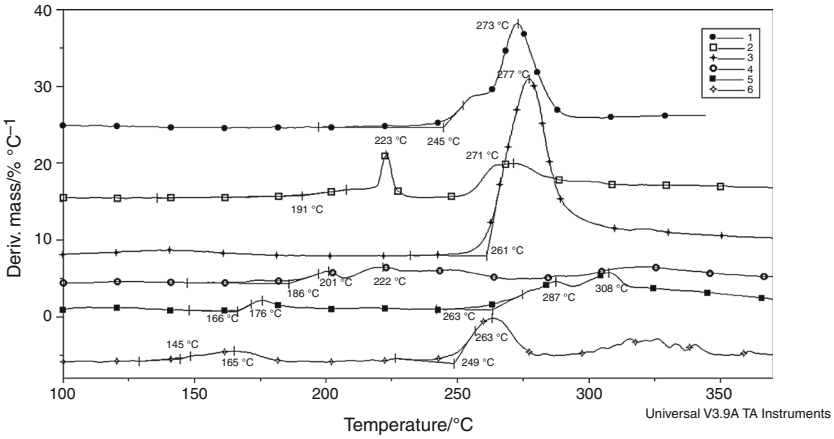

Fig. 3 DTG curves for compounds **1–6**

Scheme 1 Structure of the ligand 2-acetylpyridine *S*-methylisothiosemicarbazone

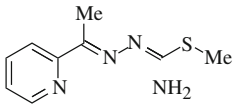

relative intensity of the peaks characteristic for thermal decomposition of **HL**, CH_3S^+: CH_3SH^+: S_2^+: $C_5H_5N^+$ are 100:61:10:6, respectively.

DTG curve with EGA–MS scan for **I** are presented in Fig. 4. Selected *m/z* values for evolved fragments are presented in Table 2 along with the corresponding data for complexes **1**, **2**, and **4–6**. As can be seen, the reaction route for **I**, proposed on the basis of simple qualitative analysis, is fully supported by TG–MS data.

The most intensive peaks present in all tested samples belong to *m/z* values of 48 and 79. The peaks appear simultaneously in the temperature range with the highest decomposition rate and are due to ligand fragmentation. In accordance with the structure of the ligand (see Scheme 1),

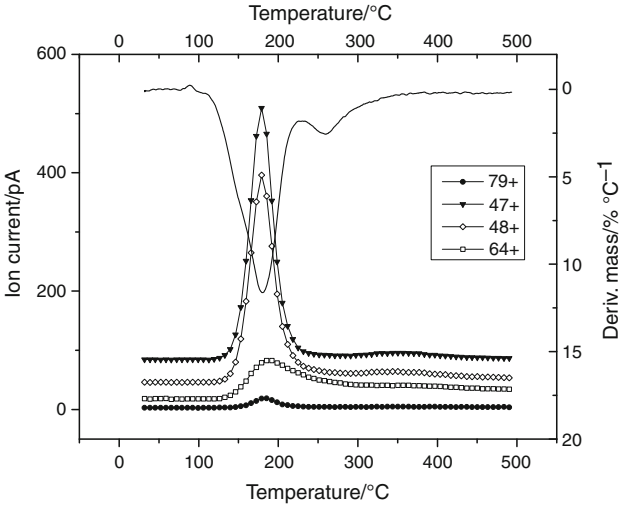

Fig. 4 DTG and simultaneous EGA–MS curves of representative ions formed during the thermal decomposition of **I** measured at a 10 °C min^{-1} heating rate in N_2 atmosphere

Table 2 Selected characteristic *m/z* data for evolved fragments with the corresponding relative intensities

m/z	Fragment	Relative peak intensity						
		HL	**1**	**2**	**4**	**5**	**6**	**I**
47	CH_3S^+	100	Signal of low intensity, not followed					
48	CH_3SH^+	61	67	100	63	95	100	85
64	S_2^+	10	22	10	30	11	23	21
79	$C_5H_5N^+$	6	100	18	100	12	42	100
35	Cl^+	–	–	–	–	–	46	5
59	$HNCS^+$	–	–	–	14	–	–	–
80	$H^{79}Br^+$	–	–	5	–	–	–	–
81	Br^+	–	–	3	–	–	–	–
127	I^+	–	–	–	–	100	–	–
128	HI^+	–	–	–	–	73	–	–
31	CH_3O^+	–	–	15	–	9	21	–
58	$C_2H_6CO^+$	–	–	–	–	–	–	32

they correspond to evolution of CH_3SH and C_5H_5N (*py*). In addition, peak with $m/z = 64$, assigned to S_2^+ evolution in **HL** decomposition, appears in the decomposition of all complexes, too.

Other characteristic signals correspond to halide ($m/z_{Cl} = 35$, $m/z_{HCl} = 36$, $m/z_{HBr} = 80$, $m/z_{Br} = 81$, $m/z_I = 127$, $m/z_{HI} = 128$) or pseudohalide ($m/z_{HNCS} = 59$) species. The decomposition of bromide compound, **2**, starts at 191 °C with methyl mercaptan and bromine formation, followed immediately by departure of *py* and S_2. The signal for $^{79}Br^+$ is superposed on $C_5H_5N^+$ signal so it is not characteristic for bromine only. The shapes and the current intensities for $H^{79}Br^+$ and $^{81}Br^+$ are about the same and reasonably significantly less than the intensity of $m/z = 79$. Compound containing iodide, **5**, decomposes at somewhat lower temperature (166 °C) with simultaneous I and HI evolution with approximately identical signal intensities. The fragmentation of the ligand occurs at around 100 °C

higher peak temperatures. The relatively slow decomposition of **4** with NCS group also starts with HNCS departure at 186 °C along with ligand fragmentation.

The desolvated **6** and **I** compounds with complex anions $[CoCl_4]^{2-}$ and $[CoCl_3py]^-$ are more stable (249 and 217 °C, respectively) compared to **2**, **4**, and **5**. Chlorine and HCl evolution start simultaneously with ligand fragmentation in both complexes. The intensity of Cl signal is significantly higher than that for HCl.

In **1** no signal characteristic for nitrate decomposition was detected. The exothermic reactions in 250–300 °C temperature range refer to oxidation of the fragments caused by nitrate. In the same temperature range, and only in complex **1**, a relative intensive peak appears with $m/z = 18$, characteristic for H_2O, thus supporting the proposition of S_2 formation instead of SO_2 evolution in **1**.

The characteristic peaks for ligand decomposition appear in all the complexes. However, the relative peak intensities vary significantly (see data in Table 2), referring to a remarkable influence of the crystal and molecular structure on the strength of individual bonds even in structurally very similar compounds, and, therefore, on their thermal decomposition pattern.

Despite the crystal solvent content in all complexes (except in **4**) the solvent peak was detected with significant intensity only in **I**, **2**, and **6** as was found by TG. It is noteworthy that in spite of the fact that crystal MeOH evaporates partially at room temperature, the evaporation peak temperatures for the rest of MeOH are in the range of 120–220 °C, which is significantly above the boiling point of MeOH (64.6 °C, 337.8 ± 0.3 K [37]). To check if the compounds **1**–**6** are stable at room temperature, the samples were dried at 40 and 60 °C to a constant mass. Dry compounds were also obtained by stepwise isothermal measurements. However, during exposure to ambient air a part of MeOH evaporates, and the compounds absorb moisture instead, giving the same mass loss after drying by repeated measurements. According to this observation, the first mass loss in compounds **1**–**6** which were stored in air for a while belongs to MeOH and/or moisture evaporation. By TG–MS measurements, signal $m/z = 18$ for water evolution was also found in all samples, but during the flashing out of the furnace, the adsorbed water evaporates at room temperature.

Antimicrobial activity

It is known that pyridine itself has a broad spectrum of biological activity [42]; therefore, the intermediate after pyridine evolution with composition of $Co_2^{III/II}L_2Cl_3$ (**II**) was isolated and also tested for antimicrobial activity. The results refer to a significantly higher activity of the organic ligand **HL** against bacteria compared to the activity of the complexes. The activity of the ligand against bacteria is comparable with those obtained for standard antibiotics (MIC, μg cm^{-3}, *E.C.* > 4, *S. A.* > 2, *B. S.* > 4, *B.C.* > 4, *M.L.* > 2) using some standard procedures for susceptibility testing by disk diffusion method [43] or dilution method in broth [44, 45]. The activity of **HL** against fungi is moderate (MIC, μg cm^{-3}, *C.A.* > 125, *A.N.* > 250).

Surprisingly, the complexes show low (**3**, MIC > 4,000; **6**, **I** and **II**: MIC > 1,000) or negligible activity against all strains, regardless of the oxidation state of Co(II or III), form of **HL** (protonated/deprotonated or both) and co-ligands, as well as the type of the counter ion, the presence/absence of crystal solvent, pH of the solution in DMSO, etc. The results could be explained by high thermodynamic and kinetic inertness of the complexes. Therefore, the liberation of the free organic ligand, central metal ions, and co-ligands is minimized. The high thermodynamic stability of the complexes is in accordance with their relatively high thermal stability (>170–250 °C).

Conclusions

The thermal behavior of seven potentially bioactive cobalt complexes with 2-acetylpyridine *S*-methylisothiosemicarbazone (**HL**) ligand containing crystal MeOH or Me_2CO was investigated by simultaneous TG/DSC measurements. The thermal data reveal that in **1**–**3** and **5**–**6** MeOH evaporates at room temperature and the samples exposed to ambient air absorb moisture, but in the absence of water vapor they are stable to above 150 °C when the decomposition of the complex begins. Acetone solvate (**I**) is surprisingly stable up to 150 °C. After the acetone departure the evaporation of pyridine takes place with 217 °C onset. The intermediate (**II**) formed after pyridine departure is stable to ~280 °C. In TG/MS spectra, the relative intensity of the peaks, characteristic for the ligand decomposition varies significantly in complexes, referring thus to the high influence of the crystal and molecular structure even in structurally similar compounds on their thermal decomposition pattern.

The activity of **HL** against bacteria is comparable with those obtained for standard antibiotics. Complexes **3**, **6**, and **I**(**II**) showed moderate activity against selected microbial strains, while the activity of the other complexes is negligible. The surprisingly low biological activity of the complexes might be explained by their high stability in solution, also supported by their relatively high thermal stability.

Acknowledgements The authors thank the Ministry of Education, Science and Technological Development of the Republic of Serbia for financial support (Project No. ON172014), and the Secretariat for

Science and Technological Development (Autonomous Province of Vojvodina, Republic of Serbia). The authors would like to thank Dr Imre Miklós Szilágyi (Department of Inorganic and Analytical Chemistry, Budapest University of Technology and Economics) for the TG–MS measurements and his valuable comments regarding the interpretation of the results. B. Holló thanks Domus Hungarica for fellowship.

References

1. CDC—2011 Annual Report: 2011 progress towards implementation of: a public health action plan to combat antimicrobial resistance.
2. Sengupta S, Chattopadhyay MK. Antibiotic resistance of bacteria: a global challenge. Resonance. 2012;17:177–91.
3. Mondelli M, Pavan F, de Souza PC, Leite CQ, Ellena J, Nascimento OR, Facchin G, Torre MH. Study of a series of cobalt(II) sulfonamide complexes: synthesis, spectroscopic characterization, and microbiological evaluation against M. tuberculosis. Crystal structure of $[Co(sulfamethoxazole)_2(H_2O)_2]\cdot H_2O$. J Mol Struct. 2013;1036:180–7.
4. Oliveri V, Viale M, Caron G, Aiello C, Gangemi R, Vecchio G. Glycosylated copper(II) ionophores as prodrugs for β-glucosidase activation in targeted cancer therapy. Dalton Trans. 2013;42:2023–34.
5. Soliman MH, Mohamed GG. Cr(III), Mn(II), Fe(III), Co(II), Ni(II), Cu(II) and Zn(II) new complexes of 5-aminosalicylic acid: spectroscopic, thermal characterization and biological activity studies. Spectrochim Acta A. 2013;107:8–15.
6. Rogolino D, Carcelli M, Sechi M, Neamati N. Viral enzymes containing magnesium: metal binding as a successful strategy in drug design. Coordin Chem Rev. 2012;256:3063–86.
7. Santos ALS, Sodre CL, Valle RS, Silva BA, Abi-chacra EA, Silva LV, Souza-Goncalves AL, Sangenito LS, Goncalves DS, Souza LOP, Palmeira VF, d'Avila-Levy CM, Kneipp LF, Kellett A, McCann M, Branquinha MH. Antimicrobial action of chelating agents: repercussions on the microorganism development virulence and pathogenesis. Curr Med Chem. 2012;19:2715–37.
8. Maheswaram MP, Mantheni D, Perera I, Venumuddala H, Riga A, Alexander K. Characterization of crystalline and amorphous content in pharmaceutical solids by dielectric thermal analysis. J Therm Anal Calorim. 2013;111:1987–97.
9. Pal S, Roopa BN, Abu K, Manjunath SG, Nambiar S. Thermal studies of furosemide–caffeine binary system that forms a co-crystal. J Therm Anal Calorim. 2013. doi:10.1007/s10973-013-3031-5.
10. Gutch PK, Jitendra S, Alankar S, Anurekha J, Ganesan K. Thermal analysis of interaction between 2-PAM chloride and various excipients in some binary mixtures by TGA and DSC. J Therm Anal Calorim. 2013;111:1953–8.
11. Wesolowski M, Rojek B. Thermogravimetric detection of incompatibilities between atenolol and excipients using multivariate techniques. Therm Anal Calorim. 2013;113:169–77.
12. Wesolowski M, Szynkaruk P, Makurat E. DSC and IR as supporting tools for identification of methylxanthines in solid dosage forms of drugs. J Therm Anal Calorim. 2012;109:807–15.
13. Magee TRA, McMinn WAM, Farrell G, Topley L, Al-Degs YS, Walker GM, Khraisheh M. Moisture and temperature dependence of the dielectric properties of pharmaceutical powders. J Therm Anal Calorim. 2013;111:2157–64.
14. Joseph J, Nagashri K, Janaki GB. Novel metal based anti-tuberculosis agent: synthesis, characterization, catalytic and pharmacological activities of copper complexes. Eur J Med Chem. 2012;49:151–63.
15. Pandya JH, Jadeja RN, Ganatra KJ. Spectral characterization and biological evaluation of Schiff bases and their mixed ligand metal complexes derived from 4,6-diacetylresorcinol. J Saudi Chem Soc. 2011. doi:10.1016/j.jscs.2011.06.010.
16. Badiger DS, Hunoor RS, Patil BR, Vadavi RS, Mangannavar CV, Muchchandi IS, Patil YP, Nethaji M, Gudasi KB. Synthesis, spectroscopic properties and biological evaluation of transition metal complexes of salicylhydrazone of anthranilhydrazide: X-ray crystal structure of copper complex. Inorg Chim Acta. 2012;384:197–203.
17. Lakshmi B, Avaji PG, Shivananda KN, Nagella P, Manohar SH, Mahendra KN. Synthesis, spectral characterization and in vitro microbiological evaluation of novel glyoxal, biacetyl and benzil bis-hydrazone macrocyclic Schiff bases and their Co(II), Ni(II) and Cu(II) complexes. Polyhedron. 2011;30:1507–15.
18. Konstantinović SS, Cakić VS. Pharmacological characteristics of some 3-salicylidenehydrazono-2-indolinone coordination compounds. Med Chem Res. 2010;19:771–81.
19. Wenzel M, Bertrand B, Eymin M-J, Comte V, Harvey JA, Richard P, Groessl M, Zava O, Amrouche H, Harvey PD, Le Gendre P, Picquet M, Casini A. Multinuclear cytotoxic metallodrugs: physicochemical characterization and biological properties of novel heteronuclear gold–titanium complexes. Inorg Chem. 2011;50:9472–80.
20. Frik M, Jiménez J, Gracia I, Falvello LR, Abi-Habib S, Suriel K, Muth TR, Contel M. Luminescent di- and polynuclear organometallic gold(I)–metal (Au_2, $\{Au_2Ag\}_n$ and $\{Au_2Cu\}_n$) compounds containing bidentate phosphanes as active antimicrobial agents. Chem Eur J. 2012;18:3659–74.
21. Milenković M, Bacchi A, Cantoni G, Radulović S, Gligorijević N, Arandelović S, Sladić D, Vujčić M, Mitić D, Anđelković K. Synthesis, characterisation and biological activity of Co(III) complex with the condensation product of 2-(diphenylphosphino)benzaldehyde and ethyl carbazate. Inorg Chim Acta. 2013;395:33–43.
22. Refat MS. Spectroscopic and thermal degradation behavior of Cr(III), Mn(II), Fe(III), Co(II), Ni(II), Cu(II) and Zn(II) complexes with thiopental sodium anesthesia drug. J Mol Struct. 2013;1037:170–85.
23. Keypour H, Shayesteh M, Rezaeivala M, Chalabian F, Elerman Y, Buyukgungor O. Synthesis, spectral characterization, structural investigation and antimicrobial studies of mononuclear Cu(II), Ni(II), Co(II), Zn(II) and Cd(II) complexes of a new potentially hexadentate N_2O_4 Schiff base ligand derived from salicylaldehyde. J Mol Struc. 2013;1032:62–8.
24. Rodić MV, Leovac VM, Jovanović LjS, Vojinović-Ješić LjS, Divjaković V, Češljević VI. Transition metal complexes with thiosemicarbazide-based ligands: part 59. Synthesis, structures and electrochemical properties of cobalt(III) complexes with 2-acetylpyridine *S*-methylisothiosemicarbazone. Polyhedron. 2012;46:124–32.
25. CrysAlisPro Software system, Version 1.171.34.36. Agilent Technologies UK Ltd., Oxford, UK.
26. Altomare A, Cascarano G, Giacovazzo C, Gualardi A. Completion and refinement of crystal structures with SIR92. J Appl Crystallogr. 1993;26:343–50.
27. Sheldrick GM. A short history of *SHELX*. Acta Crystallogr A. 2008;64:12–22.
28. Hübschle CB, Sheldrick GM, Dittrich B. ShelXle: a Qt graphical user interface for *SHELXL*. J Appl Crystallogr. 2011;44:1281–4.
29. Spek AL. Structure validation in chemical crystallography. Acta Crystallogr D. 2009;65:148–55.
30. Farrugia LJ. ORTEP-3 for Windows—a version of ORTEP-III with a Graphical User Interface (GUI). J Appl Crystallogr. 1997;30:565.

31. Finn RK. Theory of agar diffusion methods for bioassay. Anal Chem. 1957;31:975–7.
32. Lee YM, Moon JS, Yun BS, Park KD, Choi GJ, Kim JC, Lee SH, Kim SL. Antifungal activity of CHE-23C, a dimeric sesquiterpene from *Chloranthus henryi*. J Agricul Food Chem. 2009;57:5750–5.
33. Leovac VM, Češljević VI, Vojinović-Ješić LjS, Divjaković V, Jovanović LjS, Mészáros Szécsényi K, Rodić MV. Transition metal complexes with thiosemicarbazide-based ligands. Part 56. Square-pyramidal complexes of copper(II) with 2-acetylpyridine S-methylisothiosemicarbazone. Polyhedron. 2009;28:3570–6.
34. Orpen AG, Brammer L, Allen FH, Kennard O, Watson DG, Taylor R. Tables of bond lengths determined by X-ray and neutron diffraction. Part I. Bond lengths in organic compounds. J Chem Soc Perkin Trans II. 1987;S1–S19.
35. Bogdanović GA, Medaković VB, Vojinović-Ješić LjS, Češljević VI, Leovac VM, Spasojević-de Biré A, Zarić SD. Transition metal complexes with thiosemicarbazide-based ligands. Part XLI. Two crystal structures of cobalt(III) complexes with salicylaldehyde S-methylisothiosemicarbazone and theoretical study on orientations of coordinated pyridines. Polyhedron. 2001;20:2231–40.
36. Bogdanović GA, Leovac VM, Vojinović-Ješić LjS, Spasojević-de Biré A. Crystal structure of tris(pyridine)(salicylaldehyde semicarbazonato(2−))cobalt(III)-trichloropyridinecobaltate(II) at 293 and 120 K. J Serb Chem Soc. 2007;72:63–71.
37. http://webbook.nist.gov/15.05.2013.
38. Stabnikov PA, Zharkova GI, Smolentsev AI, Ukraintseva ÉA, Soldatov DV. Crystal structure and thermodynamic stability of an acetone solvate of bis(trifluoroacetylacetonato)copper(II). J Struct Chem. 2008;49:1084–9.
39. Vivekananda S, Srinivas R, Manoharan M, Jemmis ED. Generation and identification of ionic and neutral dithioformic acid [HC(S)SH], dimercaptocarbene [HSCSH], and dithiirane [H2C(S2)]: a neutralization–reionization mass spectrometry and theoretical study. J Phys Chem A. 1999;103:5123–8.
40. Gerbaux P, Flammang R, Wentrup C, Wong MW. Characterization of C_2S_4 isomers by mass spectrometry and ab initio molecular orbital calculations. Int J Mass Spectrom. 2001;210(211):31–42.
41. Eberhard J, Chen W-Ch, Yu Ch-h, Lee Y-P, Cheng B-M. Photoionization spectra and ionization energies of HSCl, HSSSH, SSCl, and HSSCl formed in the reaction system $Cl/Cl_2/H_2S$. J Chem Phys. 1998;108:6197–204.
42. Chaubey A, Pandeya SN. Pyridine: a versatile nucleuse in pharmaceutical field. Asian J Pharm Clin Res. 2011;4:5–8.
43. Bell SM, Pham JN, Nguyen TT. Antibiotic Susceptibility Testing by the CDS Method, Sixth Edition 2013, The Antibiotic Reference Laboratory, South Eastern Area Services, Randwick, Australia (http://webbook.nist.gov/). Accessed 15 May 2013.
44. Reimer LG, Stratton CW, Reller LB. Minimum inhibitory and bactericidal concentrations of 44 antimicrobial agents against three standard control strains in broth with and without human serum. Antimicrob Agents Chemother. 1981;19:1050–5.
45. Andrews JM. Determination of minimum inhibitory concentrations. J Antimicrob Chemother. 2001;48(Suppl. S1):5–16.